In Situ Gene Therapy Rescues Doxorubicin-induced Ovarian Damage via Adenovirus Mediated *Sirt1* and *Tgfbr2*

Lingwei Ma
Department of Obstetrics and Gynecology, Tongji Hospital, Tongji Medical College,Huazhong University of Science and Technology

Huan Lu
Department of Obstetrics and Gynecology, Tongji Hospital, Tongji Medical College,Huazhong University of Science and Technology

Yanzhi Feng
Department of Obstetrics and Gynecology, Tongji Hospital, Tongji Medical College,Huazhong University of Science and Technology

Yan Li
Department of Obstetrics and Gynecology, Tongji Hospital, Tongji Medical College,Huazhong University of Science and Technology

Su Zhou
Department of Obstetrics and Gynecology, Tongji Hospital, Tongji Medical College,Huazhong University of Science and Technology

Meng Wu
Huazhong University of Science and Technology

Peng-Fei Cui
National Medical Center for Major Public Health Events, Tongji Hospital, Tongji Medical College, Huazhong University of Science and Technology, Wuhan, 430000 https://orcid.org/0000-0003-2915-9157

Jinjin Zhang
Huazhong University of Science and Technology

Shixuan Wang (shixuanwang@tjh.tjmu.edu.cn)
Huazhong University of Science and Technology

Article

Keywords: chemotherapy-induced ovarian damage, AdV-Sirt1, AdV-Tgfbr2

Posted Date: September 10th, 2021

DOI: https://doi.org/10.21203/rs.3.rs-843854/v1

Abstract

Chemotherapy-induced ovarian damage and fertility loss have negative impacts on the quality of life for female cancer patients worldwide. Thus, we aimed to explore the feasibility and safety of gene therapy for prevention of such damage. First, we validated doxorubicin-induced ovarian damage in human and mouse ovarian tissues and identified two key genes (*Sirt1* and *Tgfbr2*). Next, we generated AdV-*Sirt1* and AdV-*Tgfbr2* after vectors screening (AdV,AAV and LV) for their ability to transduce mouse ovaries. Finally, we conducted *in situ* ovarian injection of AdV-*Sirt1* and AdV-*Tgfbr2* in doxorubicin-treated mice and assessed their ovarian functions and reserv*es.* The interventions dramatically alleviated doxorubicin-induced ovarian damage without apparently influencing the health status of their offspring. Together, our results indicate that AdV-*Sirt1* and AdV-*Tgfbr2* can serve as effective and safe agents for reducing doxorubicin-induced ovarian damage and also suggest that they may be potentially applicable for post-chemotherapy protection in female cancer patients.

Introduction

With the rapid progress in the diagnosis and treatment of cancer, the long-term survival rate of female patients has significantly improved [1]. Chemotherapy is an important regimen for the treatment of tumors. However, ovarian damage caused by chemotherapy is a common problem related to women's physical and mental health, including reproductive system dysplasia, premature ovarian failure, and fertility loss [2]. Hence, protecting the ovaries from chemotherapy-induced damage is crucial for female cancer patients.

Currently, some strategies that have been applied in the protection of ovarian injury caused by chemotherapy include gonadotropin-releasing hormone agonists, embryos, mature oocytes, and ovarian tissue cryopreservation and transplantation. Other approaches, such as stem cell therapy research and potential protective agents (such as AS101, AMH, and S1P), and other drugs, are still at their early developing stage [3]. Also, the application of these strategies is limited due to the complexity of technology, uncertain therapeutic effects [4,5], ethical issues, unknown risk of tumor recurrence by ovarian tissue autologous transplantation [6], narrow scope of the application, and other problems [7,8].

Gene therapy has been extensively explored for multiple tumors and genetic diseases [9]. However, the application of gene therapy for non-tumor and non-genetic abnormalities has been understudied especially in the area of ovarian damage caused by chemotherapy. Thus, in this study, we explored the feasibility and safety of gene therapy for the prevention and protection of ovarian injury caused by chemotherapy.

Doxorubicin (Dox) is a commonly used chemotherapeutic agent and also widely used for the treatment of female cancers, such as breast and ovarian cancers, and other solid tumors, in addition to hematological diseases, including leukemia, Hodgkin's lymphoma, multiple myeloma [10]. As a moderate gonadotoxic chemotherapy agent, it has been reported to cause ovarian interstitial damage, including local ovarian fibrosis and vascular damage [11–14]. However, the molecules or genes responsible for DOX-induced

ovarian damage remain incompletely understood. Thus, there is a lack of effective prevention and protection strategies for ovarian injury caused by Dox.

In our attempt to address this issue, we found that *Tgfbr2* and *Sirt1* are markedly downregulated in mouse and human damaged ovarian tissues caused by Dox. To determine whether overexpression of these two genes might be able to prevent or protect Dox-induced ovarian damage, we explored the safety, feasibility, and effectiveness of targeting *Sirt1* and *Tgfbr2* gene therapy by employing adenovirus vectors. Our results strongly indicate that these two agents effectively protect ovaries from damage caused by Dox in mice and suggest that they could be potentially useful for doxorubicin-treated cancer patients with ovarian damage.

Results

1. Doxorubicin leads to decreased ovarian reserve and declined ovarian function

Several studies have indicated that chemotherapy-induced damage to the ovary includes microvascular damage, interstitial necrosis, and fibrosis [11,15]. In our study, ovarian damage was induced by the intraperitoneal injection of doxorubicin (Dox, 10 mg kg^{-1}) (Fig. 1a). Compared with the blank group, ovarian weight and ovary index were significantly decreased (81.8% vs 25.0%, $P < 0.05$) (Fig. S1, 1b and 1c). The proportion of irregular estrus cycles increased in the Dox-treated group (Fig. 1b). The levels of estrogen, progesterone, and AMH in the Dox group decreased, and the level of follicle-stimulating hormone (FSH) was increased (Fig. 1c-f). Furthermore, the number of mouse follicles at all levels was counted after H&E staining of paraffin sections of mouse ovaries (Fig. 1g). Compared with the blank group, the number of primordial follicles (PMF), secondary follicles (SF), and total number of healthy follicles (THF) in the Dox group decreased significantly (Fig. 1h). Moreover, the proportion of primordial follicles and secondary follicles in the Dox group was lower than that in the Blank group, with atretic follicles (ATF) increasing (Fig. 1i), indicating that Dox causes a significant loss of primordial follicles and an increase in atretic follicles. In addition, fibrosis of the ovary was evaluated by red Sirius staining (Fig. 1j), showing that the proportion of collagen area in the Dox group is higher than that in the blank group (31.58% ± 1.702%, 9.975% ± 0.6826%, $P < 0.001$), which was also confirmed by polarized light photography. Masson's trichrome staining (Fig. 1k) revealed that the proportion of collagen-positive (blue) fiber area in the ovary of the Dox group is higher than that of the Dox group (3.639% ± 0.3098%, 18.59% ± 0.7567%, $P < 0.001$). The expression of the fibrosis marker α-SMA in the Dox group was higher than that in the blank group by IHC (Fig. S1, d and e). Together, these results indicate that Dox causes ovarian damage in mice by inducing ovarian interstitial fibrosis.

2. *Tgfbr2* and *Sirt1* are markedly reduced in human and mouse damaged ovarian tissues

To identify genes that might be responsible for doxorubicin-induced ovarian damage, we performed an RNA seq analysis in RNAs that were extracted from the ovarian tissues of the Dox and blank groups. Differentially expressed genes (DEGs) were obtained through data quality control, mapping, and

normalization. Compared with the blank group, the DEGs (119 upregulated genes and 178 downregulated genes) were identified in the ovaries of the Dox group compared with the blank group (FDR < 0.05, fold change > 2). The DEGs were displayed in a volcano plot (Fig. 2a) and heatmap (Fig. S2a). Gene Ontology (GO) enrichment analysis of upregulated DEGs revealed that they were mainly enriched in biological processes, such as “Adherens junction,” “Focal adhesion,” and “Extracellular matrix” (Fig. 2b). KEGG pathway enrichment analysis found that it was enriched in “ECM-receptor interaction,” “Cell adhesion molecules (CAMs),” and other pathways, indicating that Dox may increase the degree of ovarian fibrosis (Fig. S2b), which is also consistent with the ovarian phenotype in the above experiment. The genes related to steroid hormone synthesis and ovarian follicle development, such as *Hsd17b7*, *Lhcgr*, *Hmgcs1*, *and Sirt1,* were significantly downregulated, and fibrosis-related genes that inhibit fibrosis, such as *Tgfbr2* and *Mmp15*, were also downregulated (Fig. 2a). GO and KEGG pathway enrichment analysis of down-regulated genes revealed that these genes are mainly enriched in “Sterol biosynthetic process”, “Cholesterol metabolic process”, and other steroid hormone synthesis-related biology processes (Fig. 2c). KEGG pathway analysis includes “Ovarian steroidogenesis,” “Estrogen signaling pathway” and other KEGG pathways (Fig. S2c), confirming that Dox causes the decline of ovarian function. These results suggest that Dox increases the degree of ovarian fibrosis while reduces the hormone synthesis function of the ovary.

The transforming growth factor-beta 1 (*Tgfb1*) signaling pathway plays a key role in the progression of multiple organ fibrosis, such as renal fibrosis, age-related hypertrophic cardiomyopathy, immune cell recruitment, and extracellular matrix [16 17]. Exogenous administration of *Tgfbr2*-targeted inhibition of the Tgfb1 pathway can alleviate myocardial fibrosis and myocardial infarction by reducing myocardial remodeling[18], preventing the progression of heart failure, and improving the survival rate [19]. In addition, sirtuin 1 (*Sirt1*) can affect follicle development by regulating apoptosis. Studies have found that activating *Sirt1* can inhibit the activation of primordial follicles, reduce follicle assumption, and increase the reserve of follicles [20]. Therefore, it is speculated that increasing the expression of *Sirt1* can play a protective role against chemotherapy-induced ovarian damage.

Our qPCR results showed that the expression of ovarian fibrosis-related molecules *Tgfb1*, *Acta2*, *IL-1b*, *and Tnf-α* in the Dox group is upregulated, whereas the expression of *Sirt1*, *Tgfbr2*, and *Timp2* is downregulated (Fig. 2d). Western blot (WB) and immunohistochemistry (IHC) analysis revealed that the expression of *Sirt1* and *Tgfbr2* is also decreased in the Dox group (Fig. 2e and 2f). To validate the difference in the expression of *Sirt1* and *Tgfbr2* in human ovarian tissue between Dox and normal controls, 8 samples of human ovarian tissue aged between 33 and 67 years old were collected for culture *in vitro*. After culturing in medium containing Dox (1 μg mL^{-1}), the relative expression of *SIRT1* and *TGFBR2* mRNA (Fig. 2g) and protein (Fig. 2h and 2i) was significantly lower than that of the ovaries cultured in the control medium.

In summary, our results suggest that Dox might cause ovarian damage by reducing the expression of *Tgfbr2*, a key factor that inhibits the process of fibrosis, and *Sirt1* that is related to follicle development.

3. AdV serves as a suited vector for ovary infection

To identify a better vector more suited for the gene therapy experiments in ovaries, we explored the transductional tropism of three commonly used vectors by carrying out ovarian culture *in vitro* with empty viral vectors (AdV-GFP, AAV-GFP, and LV-GFP) to observe the fluorescence intensity. The results showed that AdV-GFP has a better affinity for the ovaries, as there was almost no fluorescence intensity in the LV-GFP and AAV-GFP groups (Fig. 3a and 3f). Also, the media containing 10^8, 10^9 and 10^{10} titers of AdV-GFP were used for ovarian culture *in vitro*. With time and the virus titer increased, the fluorescence also increased (Fig. 3b and 3g). The ovaries cultured with 10^{10} titer of AdV-GFP were frozen and sectioned. These samples were analyzed by GFP fluorescence and the oocyte marker Ddx4 immunofluorescence labeling (Fig. 3c). The result showed that the oocytes have almost no green fluorescence. Furthermore, the ovarian tissues were digested and separated into single cells for culture and then cultured with 10^9 empty AdV-GFP. The results showed that most of the GFP-positive cells are stroma cells, and the proportion of GFP-positive stromal cells is 61.55 ± 2.651%. The oocytes were hardly transfected (Fig. 3e and 3h). The cells were stained with Cyp17a1 (red fluorescence), a marker of ovarian stromal cells (Fig. 3d). The statistical results showed that the ratio of red light to green light overlapping cells is 52.23 ± 9.805%. These results indicate that AdV-GFP mainly infects ovarian stromal cells and has almost no infectivity to oocytes. Also, these results along with literature [21] suggest that AdV is a better gene carrier for the following ovarian gene therapy experiments.

4. Safety assessment of AdV gene therapy *in situ* injection of ovary

To further explore the safety of ovarian gene therapy and determine the duration of overexpression in the ovary, we constructed AdV-*Sirt1* and AdV-*Tgfbr2* for the following *in vivo* experiments. A schematic diagram of the vector construction is shown in Fig. 4a. The experimental flowchart is presented in Fig. 4b. The mouse ovaries of the four groups were injected with AdV-GFP, AdV-*Sirt1*, AdV-*Tgfbr2*, and PBS *in situ*, and then tested at four time points (2, 4, 6, and 8 weeks). By the end of the observation (Day 61), there was no significant difference in body weight among all of the four groups. Also, the hair color and vitality of the mice displayed no changes among the four groups. The levels of alanine aminotransferase (ALT), aspartate aminotransferase (AST), and creatine kinase (CK) were not significantly altered in each time point compared with the PBS group (Fig. 4c-e). However, blood urea nitrogen (BUN) and creatinine (CREA) in the AdV-*Sirt1* and AdV-*Tgfbr2* groups were higher than those in the PBS group at different time points (Fig. 4f-g), though the levels of the inflammation marker TNF-α in the other groups were not significantly different at various time points compared with the PBS group (Fig. 4h). Furthermore, H&E staining analyses of the hearts, livers, spleens, kidneys, and uteruses of the mice showed that there are no apparent pathological changes in these tissues (Fig. S3a). Also, there was no significant difference in organs' weights among all of the 8-week groups (Fig. S3b). By calculating the organ index, we found that there is a decrease in liver index in the AdV-*Tgfbr2* group (Fig. S3c). The changes in the liver index and the level of CREA in the AdV-*Tgfbr2* group might be due to the influence of *Tgfbr2* or other yet unknown factors, which requires further investigation.

To test whether ovarian gene therapy is toxic to the ovaries, we also tested the ovaries. There was no significant difference in the ovarian weight at each time point. AdV-*Sirt1* and AdV-*Tgfbr2* groups showed an increasing trend at 8 weeks, which may be related to the increase in body weight over time (Fig. S3d). Further calculations revealed that the ovarian index of each group did not change significantly at different time points. However, only in the AdV-*Tgfbr2* group, the 4-week group showed a significant decrease compared with the 2-week group, but it was compensated in the subsequent time (Fig. S3e). The estrous cycle of the mice in each group was monitored one week after ovarian injection *in situ* (Fig. 4i). The results showed that there is no significant difference in the ratio of regular and irregular estrous cycles among the groups (Fig. 4j). In conclusion, AdV-*Sirt1* and AdV-*Tgfbr2* appear to be safe agents because no significant damage to ovarian function in mice.

We also assessed the expression of *Sirt1* and *Tgfbr2* in mouse ovarian tissues by extracting RNAs from of ovarian tissues in each group and conducting qPCR analysis at each time point. As a result, the mRNA expression of *Sirt1* increased and lasted 2 weeks and 4 weeks after injection of AdV-*Sirt1*, but there was no significant difference by 6-8 weeks (Fig. 5a). The mRNA expression of *Tgfbr2* increased and lasted 6 weeks after injection of AdV-*Tgfbr2,* but not by week 8 (Fig. 5b). This was confirmed by WB analysis of their protein levels (Fig. 5c-f). As a control, we also detected GFP expression in mouse ovaries after injection of AdV-GFP by IHC analysis. As a result, the expression of GFP increased from 2 to 6 weeks and gradually decreased by 8 weeks (Fig. 5g-h and S4a-b). In summary, *in situ* injection of the AdV vector into the ovary can maintain the overexpression effect of target genes for 4-6 weeks.

5. The protective effects of adenovirus mediated *Sirt1* and *Tgfbr2* gene therapy on Dox-induced ovarian damage

Next, we determined whether *in vivo* restitution of *Sirt1* and *Tgfbr2* could repair or improve ovarian damage caused by Dox. As shown in Fig. 6a, mice were treated with a single dose of AdV-*Sirt1*, AdV-*Tgfbr2*, AdV-*Sirt1* combined with AdV-*Tgfbr2* or AdV-GFP control, and Dox (the model of ovarian damage was induced by the intraperitoneal injection of doxorubicin (Dox, 10 mg kg^{-1}), or N.S. control was administered intraperitoneally to the animals one week later for studying their effects on ovarian function. The animals' body weights were monitored after the intervention (Fig. S5a). Compared with their weights before surgery (day 0), the animals' body weights in each group on the first postoperative day (day 1) decreased significantly, but gradually recovered from day 2. By day 38, their body weights in the Dox, S+Dox, T+Dox, and ST+Dox groups showed a decreasing trend, compared with that of the N.S. group. The survival rate of T+Dox was 90%, and that of ST+Dox was 88.89%, showing no statistical difference when compared to the N.S., Dox, and S+Dox groups (Fig. 6b). The ovarian endocrine function and the estrous cycle of mice were monitored for 2 weeks. Interestingly, the regularity of the estrous cycle in the Dox group was 30% while the regularity of the Sirt1+Dox group increased to 44%, and the ratio of the ST+Dox group was increased to 50% (Fig. 6c and S5b). Also, sex hormone levels, such as the levels of estrogen, progesterone, and AMH, in the ST+Dox group increased significantly, compared with the Dox group. Moreover, the levels of estrogen and AMH in the T+Dox group tended to increase. There was no

significant difference in FSH levels among the five groups, but the T+Dox and ST+Dox groups showed a downward trend (Fig. 6d-g).

Compared with the Dox group, the ovarian weight of the mice in the T+Dox and ST+Dox groups were significantly increased (Fig. 6i), and the ovary index of S+Dox, T+Dox, and ST+Dox groups also increased (Fig. 6j). H&E staining of ovarian sections was performed to detect mice ovarian reserve with representative images as shown in Fig. 6h. The number of ATFs decreased in the S+Dox, T+Dox, and ST+Dox groups by follicle counting in comparison with the Dox group, (Fig. 6k). Follicle ratio results showed that compared with the Dox group, the proportion of growing follicles in the T+Dox group appeared to incline (Fig. S5d). These results suggest that AdV-*Tgfbr2* and AdV-*Sirt1*+AdV-*Tgfbr2* could improve the recovery of ovarian endocrine and reserve function after Dox treatment.

Further, we tested whether the gene therapy could improve the reproductive function of the ovary after Dox treatment. Randomly selected mice from each group were caged with wild-type male mice for 10 days, and the pregnancy rate of the female mice was tested to evaluate reproductive function. The pregnancy rates of the S+Dox, T+Dox, and ST+Dox female mice increased, compared with the Dox group (Fig. 7a). The average litter size of post-delivery mice (Fig. 7b) and all mated mice of T+Dox and ST+Dox groups (Fig. 7c) increased compared with the Dox group. There was no significant statistical difference in the average birth weight per litter (Fig. S6a) and the ratio of male to female (Fig. S6b) in each group. As shown in the representative images of the offspring of each group (Fig. 7d), all of the pups looked healthy without any apparent birth defects. These data indicate that AdV-*Tgfbr2* alone or combined with AdV-*Sirt1* via *in vivo* restitution could rescue ovarian endocrine and reproductive damage caused by Dox.

To verify whether the offspring of each group of female mice carry the AdV gene, we extracted the genomic DNA of each group of offspring mice and designed primers for the E4 region of AdV. The results of agarose gel electrophoresis after PCR showed that *Gapdh* in each group had a positive band (except for the negative control), and there was no positive band in AdV-E4 in each group (except the positive control) (Fig. 7e). This result indicates that the ovarian *in situ* injection of the AdV vector does not pass the genomic sequence of this vector to the offspring through vertical transmission. This suggests that the approach is safe to the offspring. Also, we simultaneously detected the primordial follicles and primary follicles of the ovaries in the offspring of PND3 and PND7. As shown in the representative H&E images in Fig. 7f, the number and proportion of follicles in PND3 and PND7 mice as quantified and presented in Fig. 7g and 7h were not significantly different among all of the groups, suggesting that ovarian *in situ* gene therapy does not affect the ovarian reserve of the offspring.

6. Signature transcriptome in response to overexpression of *Sirt1* and *Tgfbr2* likely underlying the protection of ovaries from doxorubicin-induced damage

To gain molecular insights into how *Sirt1* and *Tgfbr2* might improve the Dox-induced ovarian damage, we carried out transcriptome sequencing in the Dox and ST+ groups, which had a better rescuing effect. The FPKM value was obtained through quality control, mapping, and quantification. Since the gene expression value of RNA-Seq is usually expressed by FPKM, we first corrected the data and then

visualized the distribution of gene expression levels before (Fig. 8a) and after (Fig. 8b) correction through box plots, respectively. In addition, principal component analysis (PCA) was also used to assess the differences between groups and sample duplication within groups, and to perform dimensionality reduction and principal component analysis on genetic variables. The PC1 coordinate axis is the method with the largest variance in data. The PC2 coordinate axis selects the direction orthogonal to the PC1 coordinate axis and has the second largest variance. As shown in Fig. 8c, the samples were divided into two groups after PCA analysis. In order to show the correlation of gene expression between samples, Pearson correlation calculation was conducted on all gene expression levels between two samples, and the results were presented in the form of a heat map (Fig. 8d), indicating the sample differences between groups, which was used for downstream differential expressed gene (DEG) analysis. We used the Deseq2 package [22] to analyze the DEGs of the ST+Dox and Dox groups. Genes with FDR (*P.adj*) < 0.05, and log2 foldchange > 1 were extracted as DEGs. Furthermore, a heatmap plot was drawn and clustered as demonstrated in Fig. 8e. In the volcano map, some of the DEGs of interest were marked, and it was found that genes related to the fibrosis process, such as *Mmp2*, *Mmp12*, *Mmp19*, *Col22a1*, and *Timp1,* were significantly downregulated. Reproduction-related genes, such as *Fshr,* were significantly upregulated (Fig. 8f).

Table 1. GO enrichment analysis of DEGs

Category	Term	Description	Count	%	*P* value
BP	GO:0008406	gonad development	13	7.26%	1.25E-08
BP	GO:0048608	reproductive structure development	15	8.38%	2.27E-06
BP	GO:0061458	reproductive system development	15	8.38%	2.53E-06
BP	GO:0043062	extracellular structure organization	13	7.26%	1.10E-06
BP	GO:0030198	extracellular matrix organization	11	6.14%	8.81E-06
BP	GO:0046626	regulation of insulin receptor signaling pathway	6	3.35%	2.51E-05
BP	GO:1900076	regulation of cellular response to insulin stimulus	6	3.35%	6.62E-05
CC	GO:0031012	extracellular matrix	18	9.90%	3.58E-08
CC	GO:0062023	collagen-containing extracellular matrix	12	6.59%	2.57E-05
CC	GO:0030017	sarcomere	8	4.40%	0.000119391
CC	GO:0019898	extrinsic component of membrane	10	5.49%	0.000181577
CC	GO:0044449	contractile fiber part	8	4.40%	0.00019496
MF	GO:0008237	metallopeptidase activity	9	5.02%	1.08E-05
MF	GO:0004175	endopeptidase activity	13	7.26%	5.28E-05
MF	GO:0004222	metalloendopeptidase activity	6	3.35%	0.000142372
MF	GO:0046935	1-phosphatidylinositol-3-kinase regulator activity	3	1.68%	0.000164419
MF	GO:0005201	extracellular matrix structural constituent	6	3.35%	0.00086498

GO functional enrichment analysis was performed using the ClusterProfiler package [23]. The results of gene enrichment showed that in the biological process (BP) category, DEGs were significantly enriched in biological processes, such as “reproductive structure development”, “reproductive system development”, and “gonad development”. The DEGs in the cellular component (CC) category were significantly enriched

in “extracellular matrix”, “collagen-containing extracellular matrix”, collagen-containing extracellular matrix, and other cytological components. The DEGs in the molecular function (MF) category were enriched in “metallopeptidase activity” and “metalloendopeptidase activity” (Fig. 8g and Table 1). In addition, gene set enrichment analysis (GSEA) results indicated that the BP terms, such as “ovarian follicle development” and “response to gonadotropin,” in ST+Dox group were up-regulated than Dox group, and the corresponding genes of BP terms, such as *Inha*, *Inhba*, *Foxl2* and *Amh,* were ranked higher in the gene set (Fig. 8h). At the same time, the GSEA of KEGG pathway revealed that the pathways, such as “Oocyte meosis,” “Progesterone-medieated oocyte maturation,” and “Insulin signaling pathway,” in the ST+Dox group are also higher in the gene rank list. The corresponding genes *Akt1* and *Igf1r* were ranked higher in the pathway (Fig. 8i).

In addition, we used the differentially expressed pathways as the analysis object to conduct a differential pathway variation analysis (Gene set variation analysis, GSVA) [24] based on the hallmark pathway gene set provided by the molecular signature database (version 7.2) [25]. GSVA analysis showed that the term “ESTRONGEN_RESPONSE_LATE” has a higher score and that other terms, such as inflammation-related responses such as “INTERFERON_GAMMA_RESPONSE,” and “INFLAMMATORY_RESPONSE,” also have higher GSVA scores (Fig. S7a). Additionally, using the String website (https://string-db.org/) and Cytoscape (Windows 3.8.2 version), a protein-protein interaction (PPI) network of DEGs was constructed and the degree value was filtered through the Centiscape 2.2 plug-in. Genes with a degree value > 5.0 were selected as hub genes, and *Timp2* and *Mmp2* were identified as hub genes (Fig. S7b).

Discussion

Chemotherapy has been one of the commonly used cancer treatments in clinical oncology. However, it often induces ovarian damage, resulting in developmental disorders of the reproductive system, decreased ovarian reserve function, loss of fertility, and early menopause. This detrimental side effect greatly influences the self-esteem and life quality of female cancer patients before their menopause [26]. The current clinical countermeasure or potential therapies to chemotherapy-induced ovarian damage are either still at their early research phase or with unclear efficacy and possible relapse of cancer and ethical dilemmas. These negative components hinder the corresponding clinical application of these existing approaches. Hence, an effective repairing therapy is urgently needed to improve the chemotherapy-induced ovarian damage for female cancer patients.

In our study as presented, we employed a mouse model system with Dox-induced ovarian damage as a breakpoint to explore the feasibility of gene therapy as a protective strategy. The adenovirus vector was selected as a gene therapy vector in this study through screening three different gene delivery agents as further discussed below. Ovarian *in situ* injection of AdV-mediated *Sirt1* and *Tgfbr2* was used for gene therapy *in vivo*. Our findings from this set of studies demonstrated that a single administration of AdV-*Sirt1* and AdV-*Tgfbr2* individually or in combination can protect the ovarian endocrine, reproductive function, and ovarian reserve from Dox-caused damage.

First, we showed that the degree of ovarian fibrosis increases in doxorubicin-induced ovarian damage. Through RNA-Seq, we found that the expression of *Tgfbr2* and *Sirt1* decreases in the ovaries of the Dox group. Through the *in vitro* culture of human ovarian tissue in Dox, we also found that the expression of SIRT1 and TGFBR2 decreases in the human ovary. Sirt1, a longevity gene, is known to extend lifespan and delay aging [27] and plays an important role in the development of follicles [28]. In Dox-induced cardiotoxicity, the expression of *Sirt1* decreased and increased levels of apoptosis and oxidative stress; however, administration of resveratrol, a Sirt1 activator, can alleviate cardiac damage [29]. *Tgfb1* is a critical profibrotic factor, which is closely related to the synthesis of the extracellular matrix (ECM) and can cause multiple organ fibrogenesis [17]. An abnormal increase in the level of Tgfb1 in the ovary can cause follicular dysplasia and ovulation failure [30]. *Tgfbr2* specifically binds to *Tgfb1*, and exogenous administration of *Tgfbr2* can reduce the binding of *Tgfb1* to receptors on the cell membrane and subsequent signaling cascades, thereby inhibiting the process of fibrosis [18]. This study also showed that the expression of the ovarian follicle development-related gene *Sirt1* and the fibrosis-related index *Tgfbr2* decreased in the Dox-induced ovarian damage model, which is consistent with the aforementioned research in other organ systems.

Regarding the types of virus vectors, we searched the literature and summarized that the vectors that have been conducted in the germline include AAV9 [31], AdV [21 21 32 33], RV [32] and LV [32]. Based on this information, we used the empty vectors of AAV9-GFP, AdV-GFP, and LV-GFP to explore tropism to the ovary. Through *in vitro* culture of ovaries and ovarian single cells, we found that the AdV empty vector has a better tropism to the ovary, and mainly infects the stromal cells, but not the oocytes, of the ovary. Moreover, Gordon [34] reported that adenoviruses are not able to transduce female germ cells, which is a natural advantage of AdV. Therefore, AdV was selected as the vector for subsequent experiments.

AdV-*Sirt1* and AdV-*Tgfbr2* were constructed and injected into ovaries *in situ* for detection of localization, safety, and overexpression time. Two weeks after the ovarian injection *in situ*, ovarian function was not severely damaged, and the green fluorescence was mainly concentrated in the ovarian stroma, but no fluorescence was detected in the follicles, indicating that the AdV vector mainly acts on the interstitial cells of the ovary. Our results also indicated that ovarian gene therapy had no significant effect on the general health condition of the mice. The above results fully confirmed the safety of ovarian *in situ* injection of adenovirus, suitable as a carrier for gene therapy in the ovary.

AdV-*Sirt1* combined with AdV-*Tgfbr2* gene therapy showed that ovarian endocrine function and reserve function are improved in the Dox-induced mouse ovarian damage model. Investigation of reproductive function revealed that the pregnancy rate and average litter size also increase after gene therapy. Tracking down to its offspring, no offspring carrying the AdV genome was found, indicating that the adenovirus vector's own gene is not inherited by the offspring and firmly confirming the safety of gene therapy. This safety result to the reproduction system is consistent with the study using male mice as reported by Ikawa et al. [32]. *C-kit* ligand (*KL2*) gene therapy was administered to male sterile *Sl/Sl*^{d} mutant mice caused by *KL2* defects in male testicular Sertoli cells. The offspring were produced by the method

of in vitro fertilization, and no germline transduction was identified, which fully illustrates the safety of gene therapy in the male reproductive system.

In addition, we compared the histology and functional changes of mouse ovaries between the gene therapy group (AdV-*Sirt1*+AdV-*Tgfbr2*+Dox) and the chemotherapy group (AdV-GFP+Dox) through RNA-Seq. Compared with the chemotherapy group, AdV-*Sirt1* combined with AdV-*Tgfbr2* restored the structure of the reproductive system, promoted ovarian follicle development, oocyte meiosis, and maturation, and enhanced the effect of gonadotropin response.

In contrast, our RNA seq analysis of these ovarian tissues showed that genes related to the fibrosis process in DEGs are significantly downregulated. The biological processes, including extracellular matrix reorganization of the fibrosis process, metallopeptidase activity, and metallopeptidase activity, were also significantly downregulated in the gene therapy group, which confirmed that ovarian *in situ* gene therapy can alleviate ovarian fibrosis. Interestingly, the regulation of the insulin pathway ranks high in the GSEA results, which may be closely related to *Sirt1* administration and its subsequent regulation. *Sirt1* can directly or indirectly participate in the insulin signaling pathway, and can play an active role in the metabolic pathway by regulating the inflammatory response, gluconeogenesis and reactive oxygen species that promote the development of insulin resistance [35,36], which is also suggested in Fig. 8i. A number of studies showed that insulin stimulation *in vitro* of granulosa cells can promote the production of estradiol[37]. Intriguingly, Peluso [38] found that insulin administration *in vivo* can stimulate mitotic activity, but inhibit the secretion of estradiol by the ovaries. There are some contradictions between experiments *in vivo* and *in vitro* [39], indicating that the relationship between the insulin pathway and follicle development is more complicated. Our study as presented here showed that pathways related to inflammation and oxidative stress, such as interferon gamma response, reactive oxygen species pathway, and hypoxia, also score higher in GSVA, which is believed to be caused by the local inflammatory response caused by AdV vectors to the ovaries, hence, further research is still needed.

Previously, Ghadami et al. [21] used AdV-*FSHR* to perform gene augmentation therapy on *FSHR* gene knockout mouse models and showed a therapeutic effect, including enhanced oogenesis and follicle development, increased estrogen levels, and decreased serum free FSH levels. However, this research is based on the human FSHR gene C566T homozygous missense mutation transgenic knockout mice to study premature ovarian failure. Of note, this study used wild-type mice to confirm the feasibility of ovarian *in situ* injection gene therapy. However, the method of ovarian *in situ* injection used in this experiment is more complicated, so its clinical translation could be challenging. In order to express therapeutic genes in ovaries by non-surgical methods, such as intraperitoneal or intravenous injection, constructing ovarian stroma-specific promoters can be adopted in the optimization of the vector, which will be the future research direction of this research.

In summary, our study is the first to validate the feasibility of using AdV as a carrier of ovarian gene therapy, which can increase the mRNA and protein expression levels of target genes. As the method is *in situ* injection, no significant systemic damage has been detected. We also show that a single

administration of AdV-*Sirt1* with AdV-*Tgfbr2* could alleviate the damage caused by Dox to improve the ovarian endocrine, reproductive function, and ovarian reserve. Our results provide a proof of concept of using AdV-*Sirt1* with AdV-*Tgfbr2* as potential therapeutic agents for improvement of ovarian damage caused by chemotherapy, such as Dox, for female cancer patients.

Methods

1. Animal and experiment design

The 8-week-old female C57BL/6 mice used in this study were purchased from the Beijing Charles River Animal Laboratory (Beijing, China). All the mice were housed in ABSL-2 an environmentally conditioned room at 25 °C and 50% humidity with a 12-hour light/dark cycle, and given food and water ad libitum. The experimental procedures were approved by the ethics committee of Tongji hospital, Tongji Medical College, Huazhong University of Science and Technology in China.

To detect Dox-induced ovarian damage, doxorubicin (Dox) and normal saline (NS) were administered to the female mice i.p. (10 mg kg^{-1}, n=10). One week after injection, the estrous cycle was monitored for 14 days, and the mice were euthanized at diestrus. Ovaries and blood samples were collected for the following experiments.

To assess the safety and overexpression period, 100 female C57BL/6 mice were randomly divided into four groups, as described in Fig. 5a. AdV-GFP(1.0×1010 PFU mL^{-1}), AdV-*Sirt1* (6.5×10^{10} PFU mL^{-1}), AdV-*Tgfbr2* (7.0×10^{10} PFU mL^{-1}), and PBS were delivered by bilateral intraovarian injection using a Gauge 30 Hamilton syringe(5 μL, n = 25). Four groups of mice were euthanized at 2 weeks, 4 weeks, 6 weeks, and 8 weeks after the operation, and the ovaries, blood samples, and other organs were collected for further analysis.

To investigate the protective effects of ovarian function, 100 C57BL/6 mice were randomly divided into five groups, as described in Fig. 8a. Five microliters of AdV-GFP empty vector was delivered through bilateral intraovarian injection in the N.S and Dox groups, and normal saline and Dox were administered i.p. one week later. Five microliters of AdV-*Sirt1*, AdV-*Tgfbr2*, and AdV-*Sirt1* combined with AdV-*Tgfbr2* were delivered through bilateral intraovarian injection in the S+Dox, T+Dox, and ST+Dox groups, respectively, and Dox was administered i.p. one week later. After monitoring the estrous cycle for another 14 days, half of the mice were sacrificed at the stage of diestrus. The other half of the female mice was used for the mating test.

2. Surgical procedures of ovarian *in situ* injection

Sodium pentobarbital was used for anesthesia (50 mg kg^{-1} in PBS) intraperitoneally (i.p.). The mice were then placed in the prone position on a sterile gauze pad, and the limbs were stretched and fixed. The back area was shaved to expose the surgical field, and iodophor and 75% alcohol were used to disinfect the skin. A small 1 cm incision located at the dorsomedial position was made, and the peritoneal wall was

cut open using scissors. A sterile saline gauze pad was placed near the incision after finding the ovarian fat pad, exposing the ovary. Then, 5 μL of the prepared adenovirus or saline was aspirated with an alcohol-sterilized microinjection needle (30-gauge, G), and gently inserted into the bend of the fallopian tube of the ovarian sac under a stereo microscope. The needle can be observed under the ovarian sac. After injection, the ovary was returned to its initial anatomical position. The peritoneal, muscle layer, fascia, and skin were sutured with absorbable sutures. After suturing, the surgical incision was disinfected with an iodophor. The mice were placed on a heating pad for recovery to prevent hypothermia. The breathing rate and comfort level of the mice were monitored, as well as the ability to move autonomously in order to determine the postoperative recovery effect.

3. Ethical approval and human ovarian samples collection

The ovarian tissues used in this study were collected from eight patients (aged 33–67 years) at Tongji Hospital, Tongji Medical College, Huazhong University of Science and Technology. The qualifications for surgery included breast cancer, cervical spindle cell tumor, and endometrioid adenocarcinoma. The pathologists observed no abnormal ovarian pathology. The study protocol was approved by the local human research ethics committee. All patients signed an informed consent form for this study.

4. Estrous cycle monitoring

Vaginal smears were made at 9 am every day for 14 consecutive days. Dried slices were stained with hematoxylin for 5 min, rinsed with tap water three times, stained in eosin solution for half a minute, and fixed in ethanol for 10 min. The estrous cycle was identified under a light microscope by two observers, as described by Byers et al. [40].

5. Enzyme-linked immunosorbent assay

The serum levels of estrogen, progesterone, AMH, FSH, and TNF-α were measured by ELISA according to the manufacturer's instructions (Cusabio Biotech, Wuhan, China). An empty well was set up, and 50 μL of the standard solution of each concentration was added, and the samples were tested in the assay plate. Next, 50 μL of HRP-conjugate mixed solution was added to each well, excluding the empty well. This was stirred thoroughly, then the plate was sealed with a transparent film and incubated at 37℃ for 1 hour. The liquid was discarded, 200 μL of wash buffer was added to each well, and this procedure was repeated five times. Fifty microliters of substrate A and 50 μL of substrate B were pipetted into the well plate, mixed thoroughly, and incubated at 37 °C for 15 min. Then, 50 μL of stop solution was added, and the plate was read using a microplate reader (450 nm, reference 620 nm). Curve Expert 1.4 software was used to generate the standard curve and obtain the final concentration of the hormones.

6. Follicle counting

After the mouse ovaries were fixed in 4% paraformaldehyde, the tissues were embedded in paraffin and serially sectioned along the longitudinal axis of the ovary, and each section was attached to four pieces

of ovarian tissue with a thickness of 5 μm. The sections were H&E stained and counted for follicles at all stages (primordial follicles, primary follicles, secondary follicles, antral follicles, and atretic follicles) under a light microscope. The detailed morphological and structural characteristics of various levels of follicles in the mouse ovary were described by Sonigo et al. [41].

7. Histology

For H&E staining, the paraffin sections of the ovaries were deparaffinized and rehydrated by passing through dewaxing solution I (20 min), dewaxing solution II (20 min), ethanol (10 min), 95% ethanol (10 min), 80% ethanol (5 min), and 75% ethanol (5 min). The sections were stained with hematoxylin solution for 5 min, rinsed with tap water, soaked in hematoxylin differentiation solution, and rinsed with tap water. Afterwards, the sections were stained with bluing solution, rinsed with tap water, and stained with eosin dye for 5 min. The sections were dehydrated as routine procedures and sealed with neutral gum.

For immunohistochemistry, the sections were heated in a microwave for 25 min with citric acid for antigen retrieval. 3% H_2O_2 was used at room temperature to block endogenous peroxidase activity. The sections were blocked with 3% BSA for 1 h and incubated with primary antibody overnight at 4 °C. After the sections were incubated in secondary antibody (HRP labeled) for 1 h, they were stained with DAB agent and hematoxylin to visualize the signal.

For Sirius red staining, the sections were stained with Sirius red solution for 8 min and dehydrated quickly with three cycles of ethanol. Slices were placed in xylene for 5 min and mounted with neutral resin for microscopic inspection, image acquisition, and analysis.

For Masson's trichrome staining, the sections were soaked in Masson's solution overnight. Masson B and Masson C solutions were mixed at a ratio of 1:1. The sections where then soaked for 1 minute, rinsed with tap water, and differentiated for 1 minute with 1% hydrochloric acid alcohol. Subsequently, the sections were soaked in Masson D for 6 min, Masson E for 1 min, and Masson F for 2-30 s. The sections were rinsed and differentiated in 1% glacial acetic acid, dehydrated with three cups of ethanol, placed in xylene for transparency, and sealed with neutral gum. The sections were observed under a microscope and analyzed using Image Pro Plus software (version 6.0; Media Cybernetics, MD, USA).

8. Ovarian culture *in vitro*

The dissected ovaries were placed into cell culture inserts (6.5 mm, 0.4 μm, and NEST, Wuxi, China) in a 24-well plate, with 3-5 ovaries per well, and 500 μL medium was added. Minimum essential medium alpha (MEM-alpha) (Boster, Wuhan, China) was supplemented with fetal bovine serum (FBS, 3 mg mL^{-1}) (Gibco, USA), ascorbic acid (50 μg mL^{-1}) (Solarbio, Beijing, China), sodium pyruvate (0.24 mM) (Thermo Fisher Scientific, Shanghai, China), insulin-transferrin-sodium selenite media supplement (ITS, 100×) (Sigma-Aldrich, St Louis, USA), penicillin (100 U mL^{-1}), and streptomycin (100 mg mL^{-1}) (Servicebio, Wuhan, China). The protocols are described in detail in a previous study[42].

9. RNA extraction and qPCR

Total RNA was extracted from the ovaries of different groups of mice using RNAiso plus reagent (Takara, Shiga, Japan). RNA samples (1 μg) were treated with gDNA wiper mix (Vazyme, Nanjing, China) and then transcribed into cDNA using HiScript reverse transcriptase (Vazyme, Nanjing, China) according to the manufacturer's protocol. Real-time PCR was conducted using a CFX96 real-time PCR system (Bio-Rad, CA, USA). The PCR cycling parameters of the primers were as follows: pre-denaturation at 95 °C for 10 min, denaturation at 95°C for 30 s, annealing, and extension at 60°C for 30 s. The number of cycles was set to 40. Relative gene expression levels were calculated using the formula $2^{-\Delta\Delta Ct}$ with *Actb* as the endogenous control. Primer sequences are listed in Table S1.

10. Western blot

Total protein was extracted from the ovaries of the different groups by lysis buffer containing RIPA with 0.1 mM phenylmethylsulfonyl fluoride. The protein concentrations were quantified using Coomassie Brilliant G250. Proteins were separated by SDS-PAGE and transferred to a polyvinylidene fluoride membrane. After blocking in 5% nonfat milk for 1 h, the membranes were incubated with different primary antibodies (1:1000) at 4 °C overnight. The membranes were then incubated with the secondary antibody (1:3000) for 1 h at room temperature. The membranes were detected using a chemiluminescent ECL agent (Advansta, CA, USA) in a darkroom and captured using the ChemiDoc MP imaging system (Bio-Rad, CA, USA).

11. Statistical analysis

The data were analyzed using GraphPad Prism 7.0 (GraphPad Software, CA, USA) and SPSS software (version 21.0; IBM Corp., Armonk, NY, USA). Normally distributed data are presented as the mean ± standard error. Measurement data were analyzed using Student's t-test or one-way ANOVA according to the distribution condition. Count data were analyzed using the chi-square test or Fisher's exact test. Differences were considered statistically significant at $P < 0.05$; "ns' indicates not statistically different.

12. Gene expression analysis

Total RNA from frozen ovarian samples was extracted and delivered to the BGI-Wuhan lab for RNA sequencing. Clean reads were obtained after filtering the raw reads and checking the sequencing error rate and GC content distribution. HISAT software [21] was used to compare clean reads to the mouse genome assembly (GRCm38.p6). FPKM was used to display the gene expression abundance, and the corresponding annotations were added. The raw data analysis process was conducted using the BGI. Next, differentially expressed genes (DEGs) were identified using the DESeq2 package [43].The screening criteria were $|\log2(\text{FoldChange})| > 1$ and $P.adj < 0.05$. The ClusterProfiler [23] package was used for Gene Ontology (GO) [44] and KEGG [45] pathway enrichment analyses. Gene set enrichment analysis (GSEA) was performed using the ClusterProfiler package, and the reference gene set of "h.all.v7.1.symbols.gmt" in the molecular signature database [25] (version 7.2). Gene set variation analysis (GSVA) was performed using

the limma package [46] to visualize the pathways with significant differences. PPI network and hub gene identification were built using the STRING [47] database and Cytoscape software [48], with Centiscape 2.2 [49] and MCODE [50] apps.

Data availability:

The authors declare that all other data supporting the findings of this study are

available within the paper and its supplementary information files.

References

1. Brenner, H. Long-term survival rates of cancer patients achieved by the end of the 20th century: a period analysis. *Lancet* **360**, 1131–1135 (2002).
2. Molina, J. R., Barton, D. L. & Loprinzi, C. L. Chemotherapy-induced ovarian failure: manifestations and management. *Drug Saf* **28**, 401–416 (2005).
3. Spears, N. *et al.* Ovarian damage from chemotherapy and current approaches to its protection. *Hum Reprod Update* **25**, 673–693, doi:10.1093/humupd/dmz027 (2019).
4. Demeestere, I. *et al.* Gonadotropin-releasing hormone agonist for the prevention of chemotherapy-induced ovarian failure in patients with lymphoma: 1-year follow-up of a prospective randomized trial. *J Clin Oncol* **31**, 903–909, doi:10.1200/JCO.2012.42.8185 (2013).
5. Demeestere, I. *et al.* No Evidence for the Benefit of Gonadotropin-Releasing Hormone Agonist in Preserving Ovarian Function and Fertility in Lymphoma Survivors Treated With Chemotherapy: Final Long-Term Report of a Prospective Randomized Trial. *J Clin Oncol* **34**, 2568–2574, doi:10.1200/JCO.2015.65.8864 (2016).
6. Bastings, L. *et al.* Autotransplantation of cryopreserved ovarian tissue in cancer survivors and the risk of reintroducing malignancy: a systematic review. *Hum Reprod Update* **19**, 483–506, doi:10.1093/humupd/dmt020 (2013).
7. Donnez, J. & Dolmans, M.-M. Fertility Preservation in Women. *The New England journal of medicine* **377**, 1657–1665, doi:10.1056/NEJMra1614676 (2017).
8. Xiong, J. *et al.* Therapy of Endocrine Disease: Novel protection and treatment strategies for chemotherapy-associated ovarian damage. *Eur J Endocrinol*, doi:10.1530/EJE-20-1178 (2021).
9. Dunbar, C. E. *et al.* Gene therapy comes of age. *Science* **359**, 1–10, doi:10.1126/science.aan4672 (2018).
10. Blum, R. H. & Carter, S. K. Adriamycin. A new anticancer drug with significant clinical activity. *Ann Intern Med* **80**, 249–259 (1974).
11. Ben-Aharon, I. *et al.* Doxorubicin-induced ovarian toxicity. *Reprod Biol Endocrinol* **8**, 20, doi:10.1186/1477-7827-8-20 (2010).

12. Bar-Joseph, H. *et al.* Doxorubicin-induced apoptosis in germinal vesicle (GV) oocytes. *Reprod Toxicol* **30**, 566–572, doi:10.1016/j.reprotox.2010.07.003 (2010).
13. Wang, Y. *et al.* Multidrug Resistance Protein 1 Deficiency Promotes Doxorubicin-Induced Ovarian Toxicity in Female Mice. *Toxicol Sci* **163**, 279–292, doi:10.1093/toxsci/kfy038 (2018).
14. Roti Roti, E. C., Ringelstetter, A. K., Kropp, J., Abbott, D. H. & Salih, S. M. Bortezomib prevents acute doxorubicin ovarian insult and follicle demise, improving the fertility window and pup birth weight in mice. *PloS one* **9**, 1–10, doi:10.1371/journal.pone.0108174 (2014).
15. Bar-Joseph, H. *et al.* In vivo bioimaging as a novel strategy to detect doxorubicin-induced damage to gonadal blood vessels. *PloS one* **6**, e23492, doi:10.1371/journal.pone.0023492 (2011).
16. Meng, X.-M., Nikolic-Paterson, D. J. & Lan, H. Y. TGF-β: the master regulator of fibrosis. *Nat Rev Nephrol* **12**, 325–338, doi:10.1038/nrneph.2016.48 (2016).
17. Kim, K. K., Sheppard, D. & Chapman, H. A. TGF-β1 Signaling and Tissue Fibrosis. *Cold Spring Harb Perspect Biol* **10**, 1–34, doi:10.1101/cshperspect.a022293 (2018).
18. Okada, H. *et al.* Postinfarction gene therapy against transforming growth factor-beta signal modulates infarct tissue dynamics and attenuates left ventricular remodeling and heart failure. *Circulation* **111**, 2430–2437 (2005).
19. Davidsohn, N. *et al.* A single combination gene therapy treats multiple age-related diseases. *Proc Natl Acad Sci U S A* **116**, 23505–23511, doi:10.1073/pnas.1910073116 (2019).
20. Zhang, J. *et al.* Are sirtuins markers of ovarian aging? *Gene* **575**, 680–686, doi:10.1016/j.gene.2015.09.043 (2016).
21. Ghadami, M. *et al.* Toward gene therapy of premature ovarian failure: intraovarian injection of adenovirus expressing human FSH receptor restores folliculogenesis in FSHR(-/-) FORKO mice. *Mol Hum Reprod* **16**, 241–250, doi:10.1093/molehr/gaq003 (2010).
22. Love, M. I., Huber, W. & Anders, S. Moderated estimation of fold change and dispersion for RNA-seq data with DESeq2. *Genome Biol* **15**, 1–21 (2014).
23. Yu, G., Wang, L.-G., Han, Y. & He, Q.-Y. clusterProfiler: an R package for comparing biological themes among gene clusters. *OMICS* **16**, 284–287, doi:10.1089/omi.2011.0118 (2012).
24. Hänzelmann, S., Castelo, R. & Guinney, J. GSVA: gene set variation analysis for microarray and RNA-seq data. *BMC Bioinformatics* **14**, 7, doi:10.1186/1471-2105-14-7 (2013).
25. Subramanian, A. *et al.* Gene set enrichment analysis: a knowledge-based approach for interpreting genome-wide expression profiles. *Proc Natl Acad Sci U S A* **102**, 15545–15550 (2005).
26. Ahmad, S. S., Reinius, M. A., Hatcher, H. M. & Ajithkumar, T. V. Anticancer chemotherapy in teenagers and young adults: managing long term side effects. *BMJ (Clinical research ed.)* **354**, 1–8, doi:10.1136/bmj.i4567 (2016).
27. Chang, K. T. & Min, K.-T. Regulation of lifespan by histone deacetylase. *Ageing Res Rev* **1**, 313–326 (2002).

28. Iljas, J. D., Wei, Z. & Homer, H. A. Sirt1 sustains female fertility by slowing age-related decline in oocyte quality required for post-fertilization embryo development. *Aging Cell* **19**, doi:10.1111/acel.13204 (2020).
29. Ruan, Y. *et al.* SIRT1 suppresses doxorubicin-induced cardiotoxicity by regulating the oxidative stress and p38MAPK pathways. *Cell Physiol Biochem* **35**, 1116–1124, doi:10.1159/000373937 (2015).
30. Zhou, F., Shi, L.-B. & Zhang, S.-Y. Ovarian Fibrosis: A Phenomenon of Concern. *Chinese medical journal* **130**, 365–371, doi:10.4103/0366-6999.198931 (2017).
31. Kano, M. *et al.* AMH/MIS as a contraceptive that protects the ovarian reserve during chemotherapy. *Proc Natl Acad Sci U S A* **114**, E1688-E1697, doi:10.1073/pnas.1620729114 (2017).
32. Ikawa, M. *et al.* Restoration of spermatogenesis by lentiviral gene transfer: offspring from infertile mice. *Proc Natl Acad Sci U S A* **99**, 7524–7529 (2002).
33. Kanatsu-Shinohara, M. *et al.* Adenovirus-mediated gene delivery and in vitro microinsemination produce offspring from infertile male mice. *Proc Natl Acad Sci U S A* **99**, 1383–1388 (2002).
34. Gordon, J. W. Direct exposure of mouse ovaries and oocytes to high doses of an adenovirus gene therapy vector fails to lead to germ cell transduction. *Molecular therapy* **3**, 557–564, doi:10.1006/mthe.2001.0290 (2001).
35. Cao, Y. *et al.* SIRT1 and insulin resistance. *J Diabetes Complications* **30**, 178–183, doi:10.1016/j.jdiacomp.2015.08.022 (2016).
36. Wang, R.-H. *et al.* Hepatic Sirt1 deficiency in mice impairs mTorc2/Akt signaling and results in hyperglycemia, oxidative damage, and insulin resistance. *The Journal of clinical investigation* **121**, 4477–4490, doi:10.1172/JCI46243 (2011).
37. Kolodziejczyk, J., Gertler, A., Leibovich, H., Rzasa, J. & Gregoraszczuk, E. L. Synergistic action of growth hormone and insulin-like growth factor I (IGF-I) on proliferation and estradiol secretion in porcine granulosa and theca cells cultured alone or in coculture. *Theriogenology* **60**, 559–570 (2003).
38. Peluso, J. J., Delidow, B. C., Lynch, J. & White, B. A. Follicle-stimulating hormone and insulin regulation of 17 beta-estradiol secretion and granulosa cell proliferation within immature rat ovaries maintained in perifusion culture. *Endocrinology* **128**, 191–196 (1991).
39. Poretsky, L., Cataldo, N. A., Rosenwaks, Z. & Giudice, L. C. The insulin-related ovarian regulatory system in health and disease. *Endocr Rev* **20**, 535–582 (1999).
40. Byers, S. L., Wiles, M. V., Dunn, S. L. & Taft, R. A. Mouse Estrous Cycle Identification Tool and Images. *PLOS ONE* **7**, e35538, doi:10.1371/journal.pone.0035538 (2012).
41. Sonigo, C. *et al.* High-throughput ovarian follicle counting by an innovative deep learning approach. *Scientific Reports* **8**, 13499, doi:10.1038/s41598-018-31883-8 (2018).
42. Au - Komatsu, K., Au - Iwase, A., Au - Murase, T. & Au - Masubuchi, S. Ovarian Tissue Culture to Visualize Phenomena in Mouse Ovary. *JoVE*, e57794, doi:doi:10.3791/57794 (2018).

43. Love, M. I., Huber, W. & Anders, S. Moderated estimation of fold change and dispersion for RNA-seq data with DESeq2. *Genome Biol* **15**, 550 (2014).
44. Gene Ontology Consortium: going forward. *Nucleic Acids Res* **43**, D1049-D1056, doi:10.1093/nar/gku1179 (2015).
45. Kanehisa, M. *et al.* KEGG for linking genomes to life and the environment. *Nucleic Acids Res* **36**, D480-D484, doi:10.1093/nar/gkm882 (2008).
46. Ritchie, M. E. *et al.* limma powers differential expression analyses for RNA-sequencing and microarray studies. *Nucleic Acids Res* **43**, e47-e47, doi:10.1093/nar/gkv007 (2015).
47. von Mering, C. *et al.* STRING: a database of predicted functional associations between proteins. *Nucleic Acids Res* **31**, 258–261 (2003).
48. Shannon, P. *et al.* Cytoscape: a software environment for integrated models of biomolecular interaction networks. *Genome Res* **13**, 2498–2504 (2003).
49. Scardoni, G., Petterlini, M. & Laudanna, C. Analyzing biological network parameters with CentiScaPe. *Bioinformatics* **25**, 2857–2859, doi:10.1093/bioinformatics/btp517 (2009).
50. Bader, G. D. & Hogue, C. W. V. An automated method for finding molecular complexes in large protein interaction networks. *BMC Bioinformatics* **4**, 1–27 (2003).

Declarations

Acknowledgments

Funding:

National Natural Science Foundation of China 81873824 (SW)

National Natural Science Foundation of China 82001498 (JZ)

National Natural Science Foundation of China 82002768 (PC)

Clinical Research Pilot Project of Tongji hospital, Huazhong University of Science and Technology 2019CR205 (SW)

Author contributions:

Conceptualization: JZ, SW

Methodology: JZ, SW

Investigation: LM, HL, YF

Visualization: LM, HL, YF

Supervision: YL, SZ, MW, PC

Writing—original draft: LM, HL

Writing—review & editing: YL, SZ, MW, JZ, SW

All authors have read and approved the final manuscript.

Competing interests: Authors declare that they have no competing interests.

Materials & Correspondence: Corresponding authors' Email:

shixuanwang@tjh.tjmu.edu.cn (S. W.);

jinjinzhang@tjh.tjmu.edu.cn (J. Z.)

Figures

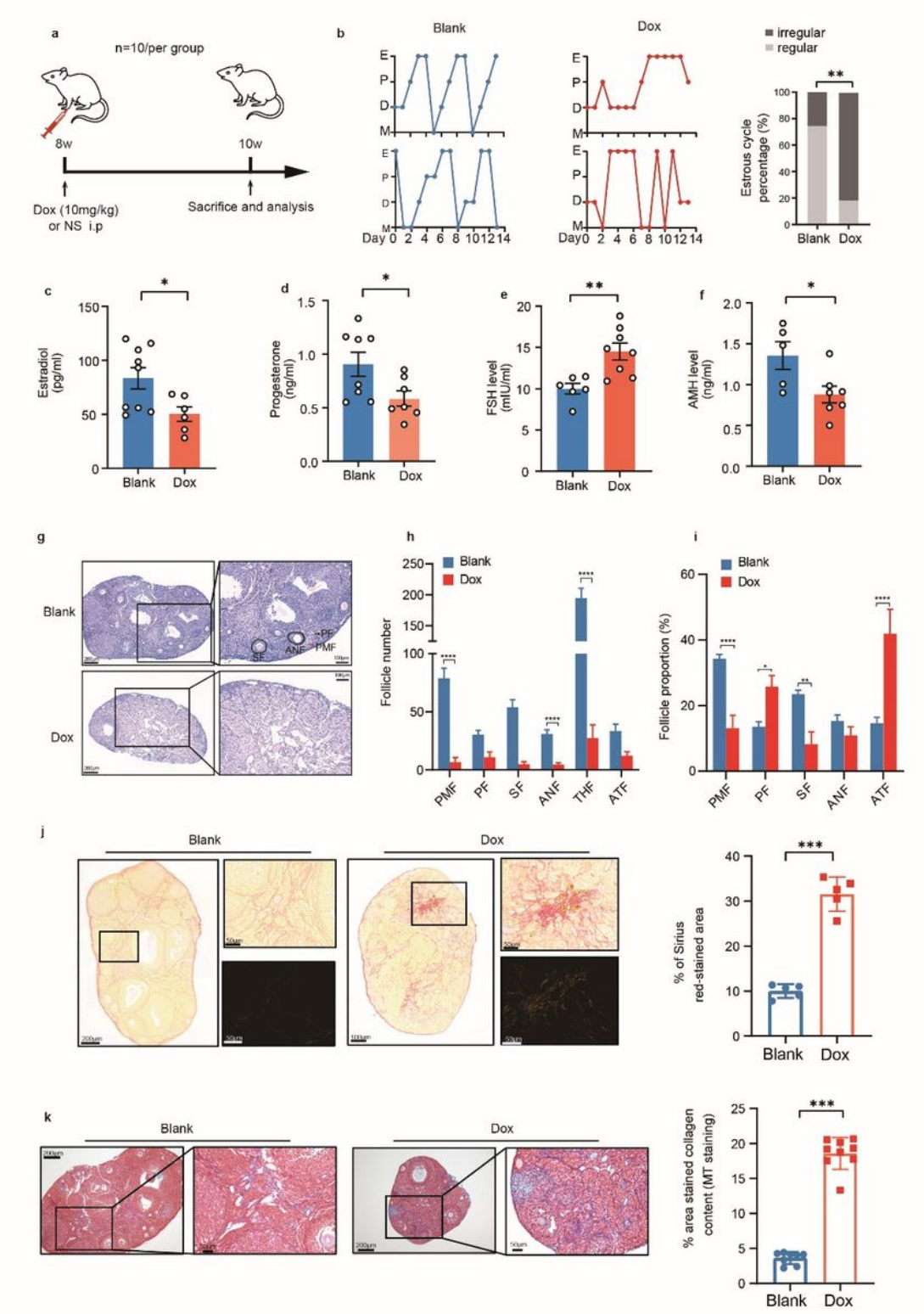

Figure 1

Doxorubicin impairs ovarian function and reserve. a Schematic diagram of the animal experiment design to detect the effect of doxorubicin (Dox) on ovarian endocrine function and ovarian reserve. NS, normal saline. b The representative estrous cycle monitoring of Blank and Dox group mice and the proportion of regular or irregular estrous cycle of Blank and Dox group mice. Levels of serum estrogen (c), progesterone (d), FSH (e) and AMH (f) in control mice and mice with Dox treatment. g Hematoxylin-eosin (HE) stained

sections of con and Dox-treated mice ovaries. Follicle counting (h) and follicle proportion (i) results based on H&E-stained ovarian serial sections. j Sirius red stained sections of con and Dox-treated mice ovaries and the statistical analysis on the right. k Masson's trichrome (MT) staining of con and Dox-treated mice ovaries. MT stained collagen content area proportion on the right. PMF: primordial follicles, PF: primary follicles, SF: secondary follicles, ANF: antral follicle, THF: total healthy follicle, ATF: atretic follicle. * P < 0.05, ** P < 0.01, *** P < 0.001.

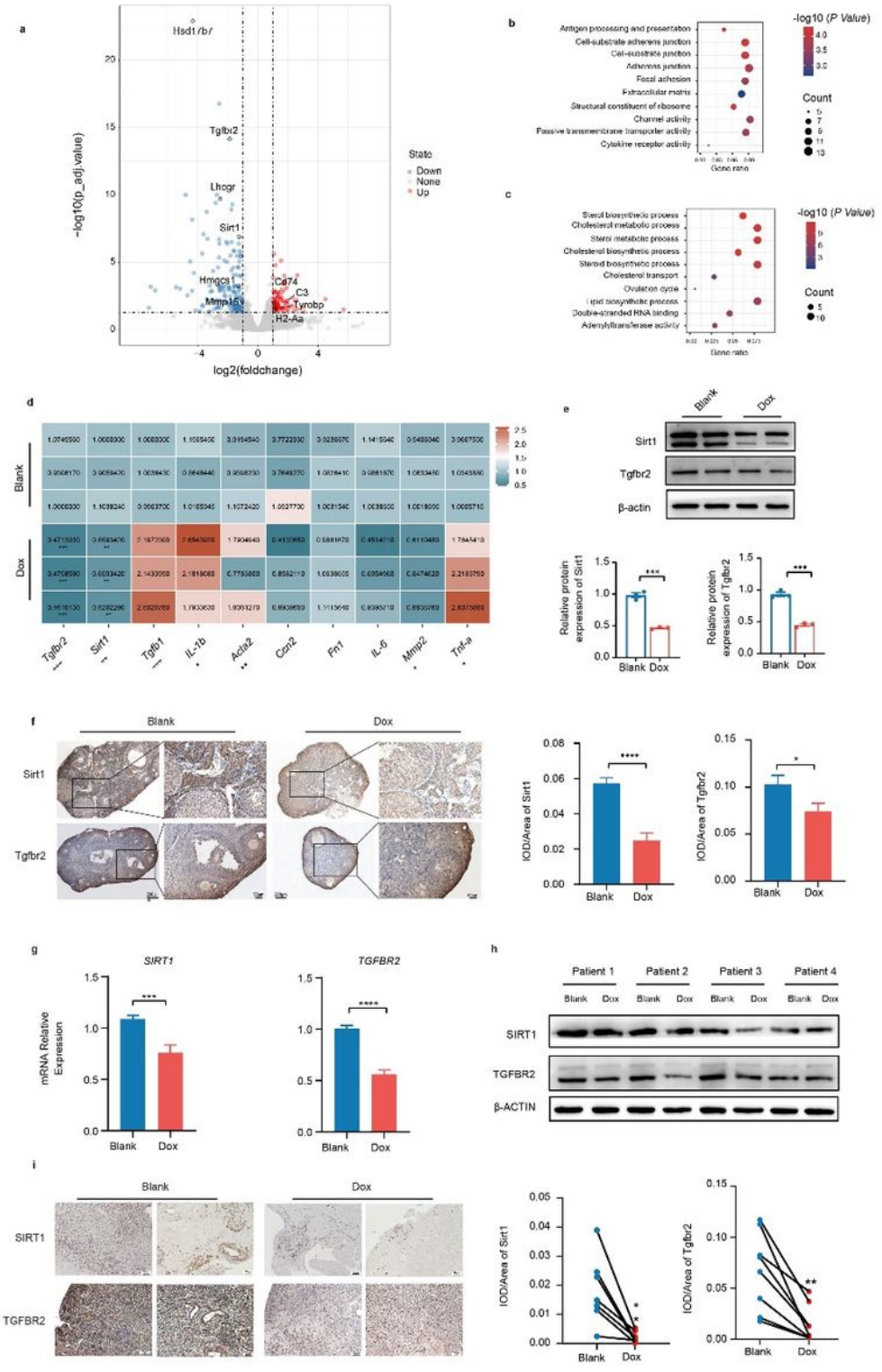

Figure 2

Identification of Sirt1 and Tgfbr2 as two genes dramatically changes in Dox-treated ovaries through screening and validation. a Volcano plot of blank and Dox-treated groups. GO enrichment analysis of DEG of upregulated (b) and down-regulated (c) DEGs in Dox-induced ovarian damage. d The mRNA level changes of related genes in the ovaries by qPCR of Blank and Dox groups of mice. The gradient color from blue to red indicates the change in expression value from low to high. e Western Blot detects the changes in the expression of Tgfbr2 and Sirt1 in the ovaries of Blank and Dox groups of mice, and the relative protein expression of Sirt1 and Tgfbr2. f IHC detection of Sirt1 and Tgfbr2 protein expression in the ovaries of the Blank and Dox groups. Typical images on the left, relative expression level analysis of Sirt1 and Tgfbr2 on the right. g The change in the mRNA level in SIRT1 and TGFBR2 in human ovarian tissues cultured in vitro. h The change in protein level in SIRT1 and TGFBR2 in human ovarian tissues by WB in Blank and Dox groups. i Representative images of IHC detection of SIRT1 and TGFBR2 expression in human ovarian tissues in Blank and Dox group on the left. The relative expression level analysis of SIRT and TGFBR2 on the right. * $P < 0.05$, ** $P < 0.01$, *** $P < 0.001$, ****$P < 0.0001$.

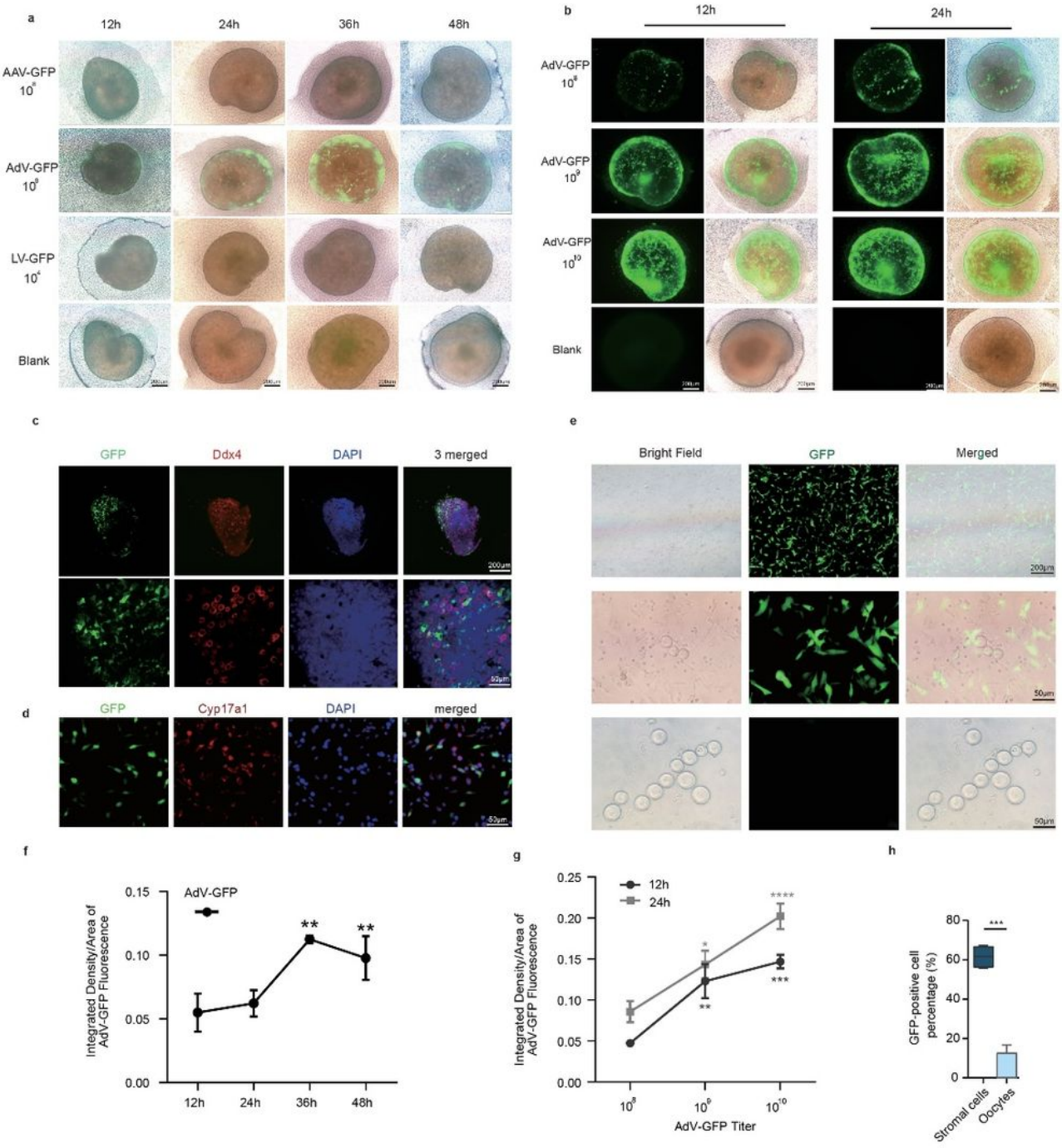

Figure 3

The comparison of AdV, AAV9 and LV empty vectors in their ability to infect ovaries in vitro. a Typical fluorescence images of the ovaries cultured in medium containing AdV-GFP (108), AAV9-GFP (108) and LV-GFP (104) from 12h to 48h. b Typical fluorescence image of the ovarian cultured in medium containing different titers of AdV-GFP (108, 109 and 1010). c Auto fluorescence (GFP) and immunofluorescence staining with Ddx4 (RFP) after frozen section. d Auto fluorescence (GFP) and

immunofluorescence staining with Cyp17a1 (RFP) in ovarian cells containing AdV-GFP (109). e Bright, GFP and merged field of view of ovarian cells cultured in a medium containing 109 titers of AdV-GFP (109) vector for 24h. f The relative fluorescence density analysis of AdV-GFP over time. g The relative fluorescence density analysis of different titers of AdV-GFP. h GFP-positive cell percentage of stromal cells and oocytes. * P < 0.05, ** P < 0.01, *** P < 0.001, ****P < 0.0001.

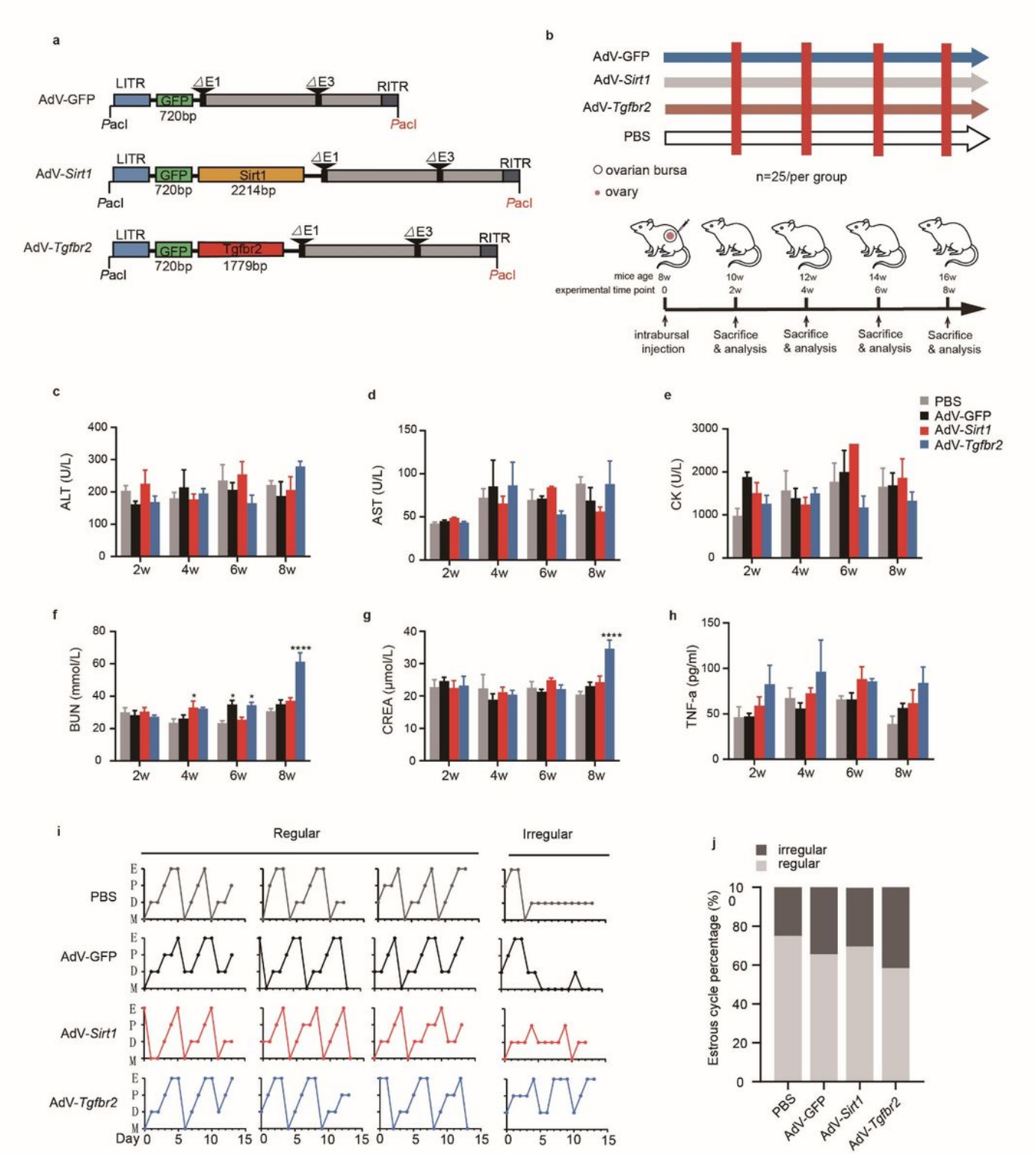

Figure 4

Ovarian in situ injection of AdV-Sirt1 and AdV-Tgfbr2 does not affect blood biochemistry and ovarian function of mice. a Schematic diagram of AdV-GFP, AdV-Sirt1 and AdV-Tgfbr2. b Schematic diagram of the animal experiment design to assess the safety of ovarian gene therapy. Serum biochemical profiles at each time in each group: ALT (c), AST (d), CK (e), BUN (f), CREA (g), TNF-α (h). i Typical line charts of estrous cycle changes in each group. j The proportion of regular and irregular estrous cycle. P: proestrus stage, E: estrus stage, M: metestrus stage; D: diestrus stage. * P < 0.05, ** P < 0.01, *** P < 0.001, ****P < 0.0001.

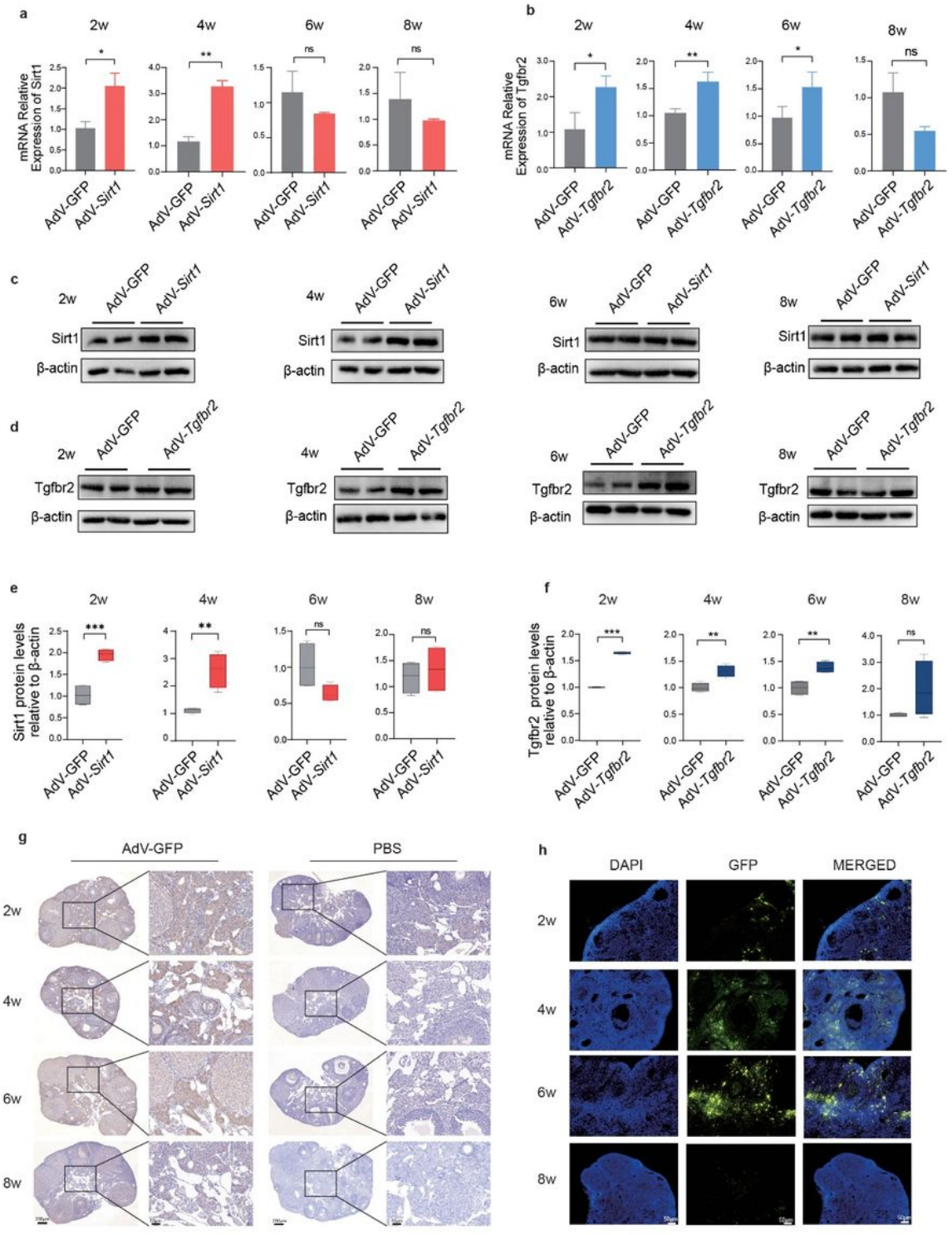

Figure 5

Expression of Sirt1 and Tgfbr2 in ovaries after AdV in situ injeciton. a The mRNA expression level of Sirt1 in AdV-GFP group and AdV-Sirt1 group from 2w to 8w over time. b The mRNA expression level of Tgfbr2 in AdV-GFP group and AdV-Tgfbr2 group from 2w to 8w over time. c The protein expression level of Sirt1 in AdV-GFP group and AdV-Sirt1 group from 2w to 8w over time. d The protein expression level of Tgfbr2 in AdV-GFP and AdV-Tgfbr2 group from 2w to 8w over time. e The relative protein expression analysis of Sirt1. f The relative protein expression level of Tgfbr2. g Representative images of IHC detection of GFP expression in AdV-GFP group and PBS group over time. h Representative images of the expression of GFP in AdV-GFP group of by detection of frozen sections. * $P < 0.05$, ** $P < 0.01$, *** $P < 0.001$, ****$P < 0.0001$.

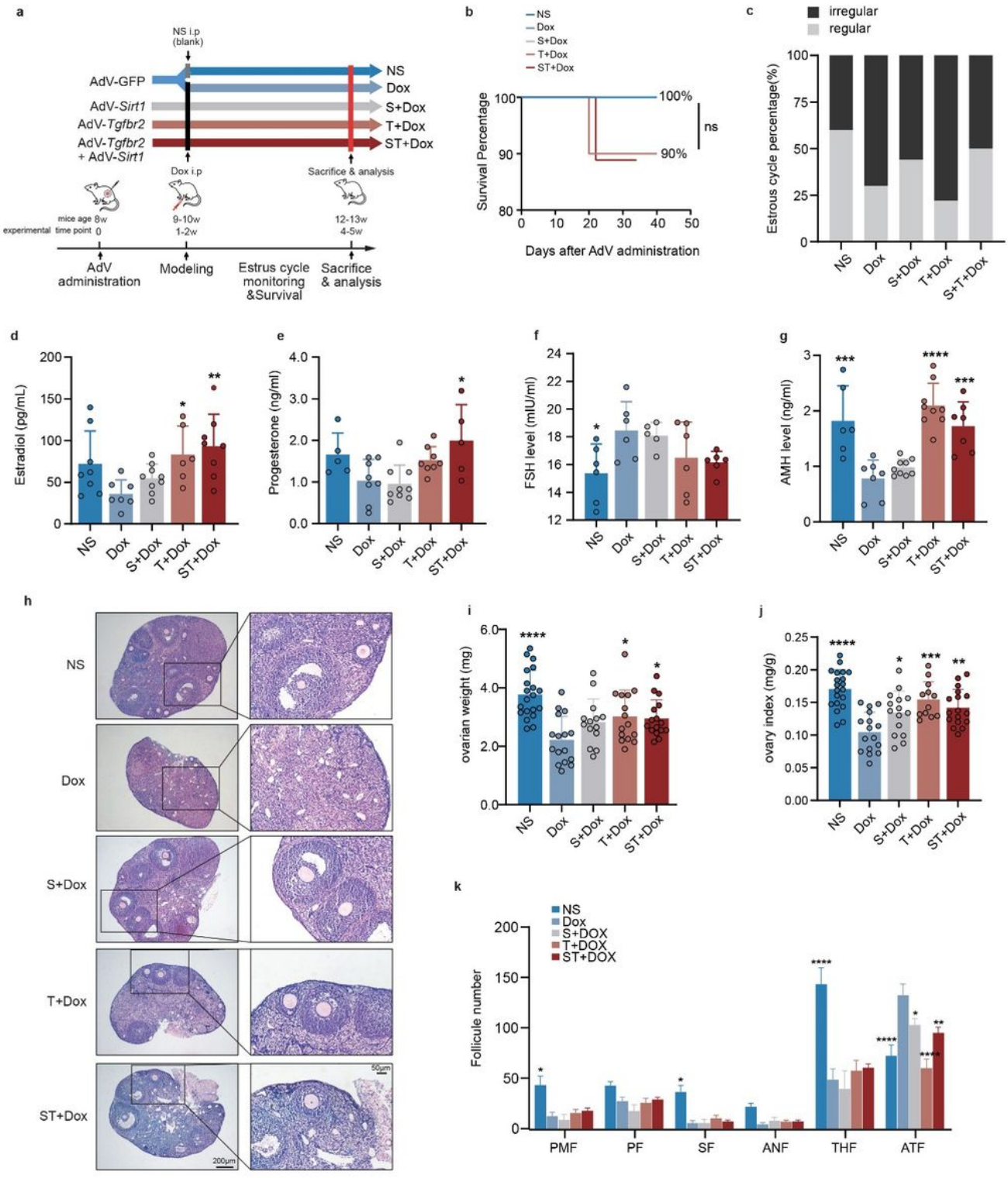

Figure 6

AdV-Sirt1 and AdV-Tgfbr2 alleviate Dox-induced ovarian damage. a Schematic diagram of the animal experiment design to explore the preventive and therapeutic effects of ovarian gene therapy on ovarian damage caused by Dox. b The survival percentage of NS group, Dox group, S+Dox group, T+Dox group and ST+Dox group. c The ratio of regular and irregular estrous cycle of each group. d The estrogen level of mice in each group. e The progesterone level of mice in each group. f The FSH level of mice in each

group. g The AMH level of mice in each group. h Representative images of H&E stained sections of mice ovaries. Changes in ovarian weight (i) and ovary index (j) of each group. (k) Ovarian follicle number based on ovarian sections in each group. * P < 0.05, ** P < 0.01, *** P < 0.001, ****P < 0.0001. P: proestrus stage, E: estrus stage, M: metestrus stage; D: diestrus stage.

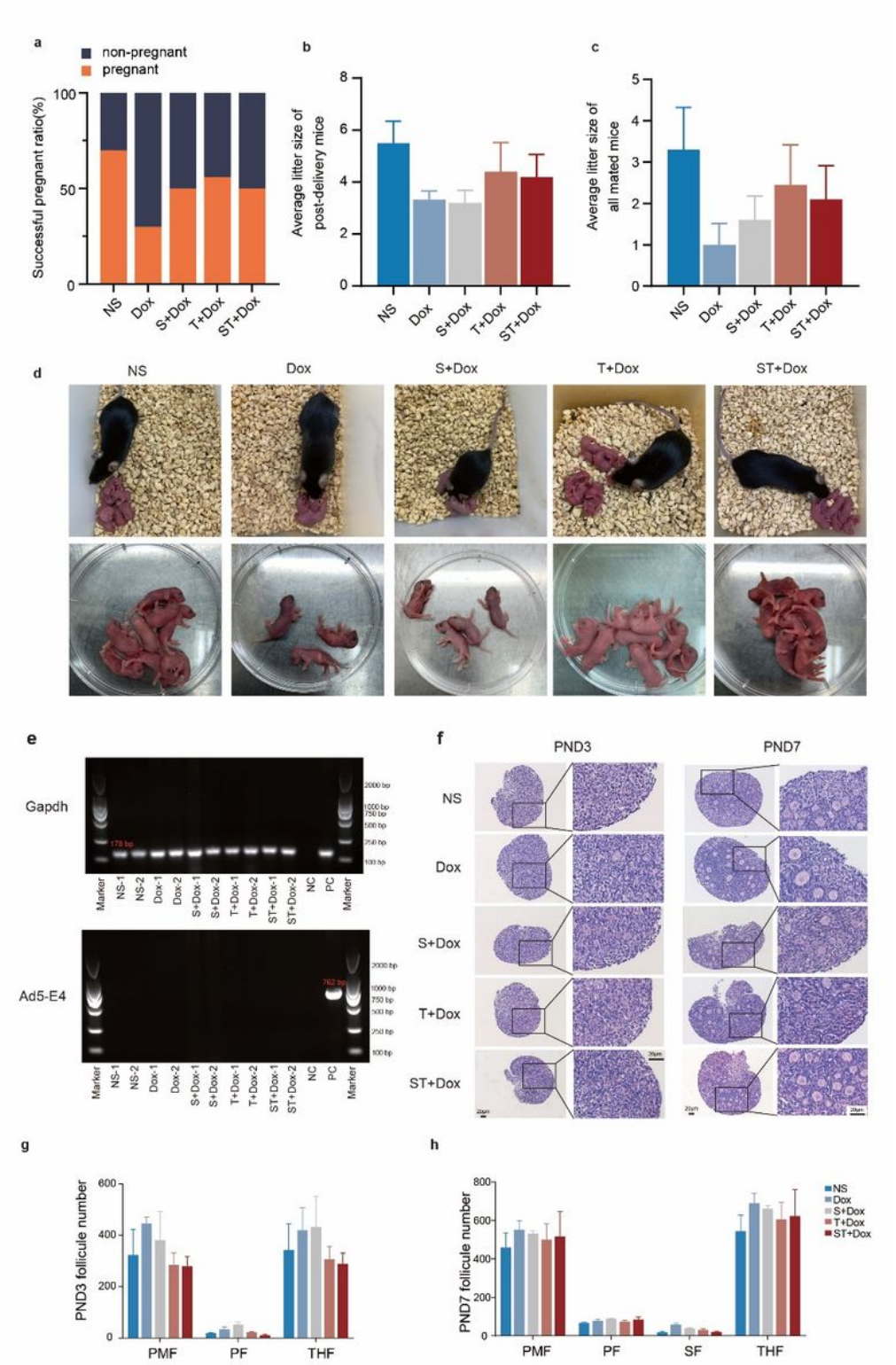

Figure 7

Effects of AdV-Sirt1 and AdV-Tgfbr2 on the reproductive function of ovaries upon Dox-induced damage. a The pregnancy ratio of each group. b The average litter size of postpartum female mice of each group. c The average litter size of all mated female mice of each group. d Typical images of postpartum female mice and their offspring in each group. e There is no vertical transmission of AdV in the offspring. The expression of Gapdh on the top. The expression of AdV5-E4 gene on the bottom. NC: Negative control, PC: positive control. f Typical H&E stained images of postnatal day (PND) 3 and PND7 in each group. Follicle counts of PND3 (g) and PND7 (h) ovaries. PMF: primordial follicles, PF: primary follicles, SF: secondary follicles, THF: total healthy follicles.

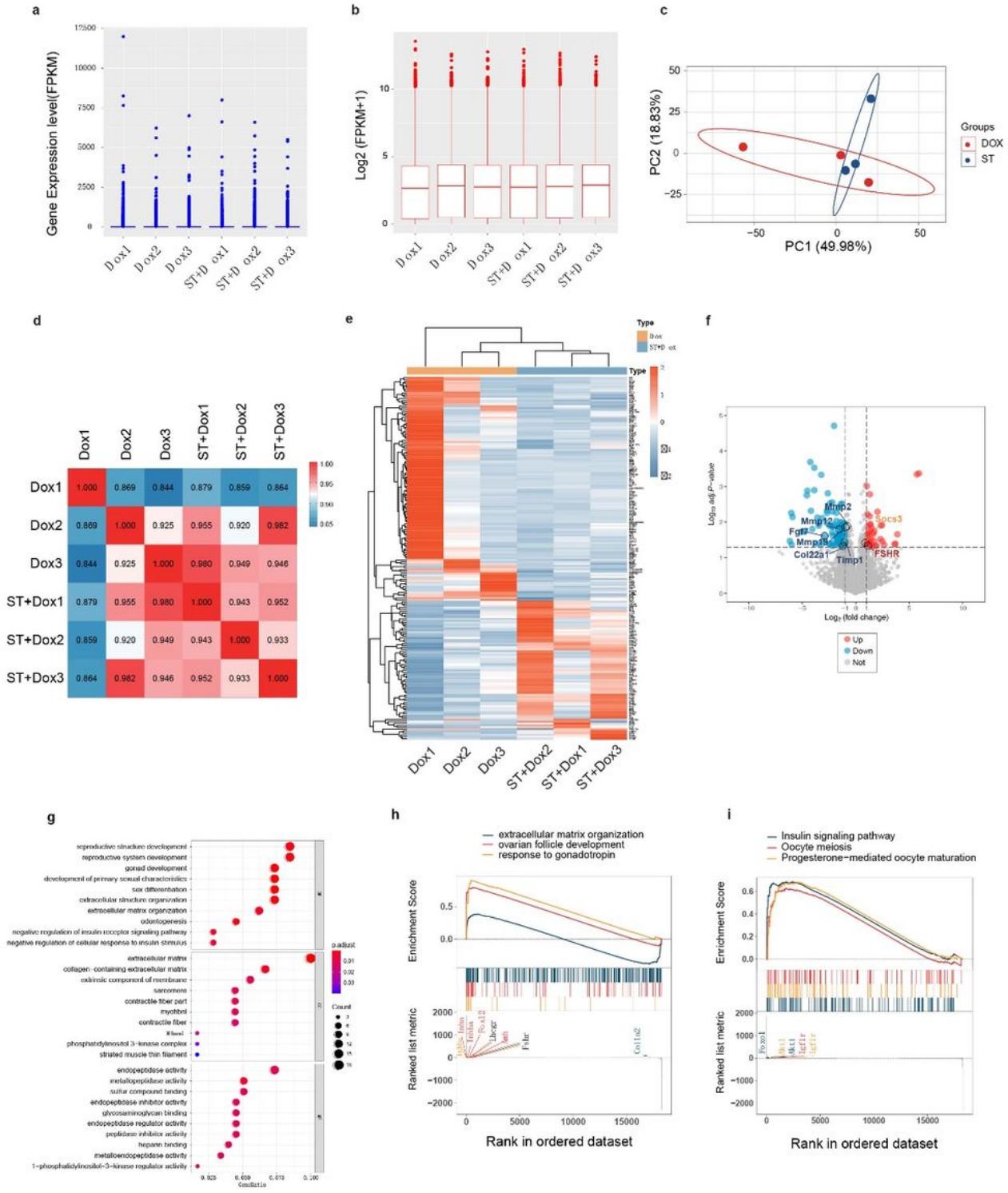

Figure 8

The comparison of gene expression profiling in ovaries between the Dox and ST+Dox groups. a Box plot before data normalization. b Box plot after data normalization. (Each box plot corresponds to 5 statistics: from top to bottom are the maximum value, the upper quartile, the median, lower quartile and the minimum value). c The principal component analysis plot of Dox and ST+Dox. d Correlation analysis of each group of the ovarian samples, the color of the number corresponds to the legend rule on the right. e

Heatmap visualization of the DEGs in Dox and ST+Dox ovarian tissues. The gradual process of color from red to blue indicates the change of expression value from high to low. f Volcano map shows the DEGs in the ovarian tissues of Dox and ST+Dox group. Red: significantly up-regulated genes, blue: significantly down-regulated genes, grey: non-significantly different genes. g GO functional enrichment of DEGs. h GSEA results of GO terms. (i) GSEA results of KEGG pathway enrichment.

Supplementary Files

This is a list of supplementary files associated with this preprint. Click to download.

- SupplementaryMaterials.docx